Micro and Nanocrystalline $LuPO_4$(Ln^{3+}: Nd, Pr) — Morphology, Luminescence and Inter-ionic Interplays

O. Bezkrovna[a,b,*], P. Zdeb[a], O. Bezkrovnyi[a], R. Lisiecki[a] and P.J. Dereń[a]

[a] *Institute of Low Temperature and Structure Research, Polish Academy of Sciences, Okólna 2, 50-422 Wrocław, Poland*
[b] *Institute for Single Crystals, NAS of Ukraine, Nauky Ave. 60, 61001, Kharkiv, Ukraine*

Received: 07.06.2023 & Accepted: 30.08.2023

Doi: 10.12693/APhysPolA.144.263 *e-mail: o.bezkrovna@intibs.pl

The effect of dopants (Nd^{3+}, Pr^{3+}) introduced into micro and nanocrystals of $LuPO_4$ on their structural, morphological, and luminescent properties has been examined. The tetragonal structure of the synthesized phosphates was confirmed by means of an X-ray diffraction study. Transmission electron microscopy of $LuPO_4$ samples doped with 0–2% Pr^{3+} and 0–3% Nd^{3+} obtained by the microwave hydrothermal method showed the formation of the nanocrystalline samples with a size of 40–90 nm. Spectroscopic study of $Lu_{1-x-y}Pr_xNd_yPO_4$ micro and nanocrystals showed that effective energy transfer occurs between the selected optically active ions. Due to significant ion–ion interactions in the co-doped orthophosphates, the contribution of nonradiative processes to the relaxation of the luminescent levels of praseodymium and neodymium effectively increases. The energy transfer in the micro and nanocrystals $Lu_{1-x-y}Pr_xNd_yPO_4$ from Pr^{3+} ions to Nd^{3+} ions results in the efficient near-infrared emission in the region of the spectrum between 1064 and 1350 nm, whereas for $Lu_{1-x-y}Pr_xNd_yPO_4$ nanocrystals doped with Pr^{3+} and Nd^{3+} ions, a particularly intense Nd^{3+} luminescence appears at 1064 nm. There is a significant impact of concentration of the Pr^{3+} and Nd^{3+} ions on near-infrared luminescence intensity of the studied $Lu_{1-x-y}Pr_xNd_yPO_4$ phosphates. The relaxation dynamic of the neodymium metastable excited state is substantially sensitive to a variety of praseodymium admixtures, and inversely, the experimental lifetime of $^1D_2$ Pr^{3+} emission level gradually decreases with increasing Nd^{3+} concentration.

topics: lutetium phosphate, microcrystals, nanocrystals, luminescent properties

1. Introduction

Rare earth (RE) ions are effective dopants for the host of phosphors and are very useful for creating materials with luminescence and upconversion properties [1–8]. Luminescent nanoparticles doped with Pr^{3+} [9] and Nd^{3+} [10] activator ions have been synthesized for use as a multi-range optical sensor of temperature. Rare earth orthophosphates (especially lutetium phosphate) can be considered excellent hosts for Ln^{3+} ions [1–7]. Phosphates possess high emission efficiency, excellent thermal and chemical stability, photostability, and high quantum emission yields. The ability to tune emission wavelengths, high brightness levels, and long emission lifetime make them a promising alternative luminescent carrier for a wide range of applications in biotechnology and biomedicine [5, 11, 12], and luminescent temperature [13] and pressure [14] sensors.

It is known that rare-earth phosphates, which include lutetium phosphate, can be used as stable matrices for the introduction of luminescent ions of trivalent lanthanide ions [5]. The low toxicity of phosphates and the possibility of using the nanoparticles based on $LuPO_4$ as nanoprobes for optical imaging and computed tomography allow them to be used for biomedical purposes. Furthermore, orthophosphates can be used to form transparent colloidal solutions with upconversion properties with possible applications in luminescent markers, imaging, and displays in fluid media [7], scintillator materials [15], multifunctional up-converting and down-converting nanomaterials excited by the ultraviolet (UV) and near-infrared (NIR) radiation [1, 16]. Lutetium orthophosphates can be made with controlled size, shape, and dopant concentration of RE ions. The nanoparticle sizes and morphology of nanocrystals can be controlled and stabilized by adding the organic molecules (cetyl-trimethyl ammonium bromide (CTAB, $C_{19}H_{42}BrN$) [2]), citric acid [5], and other compounds.

The luminescent nanoparticles can be synthesized in many different ways. There are sol–gel synthesis [17, 18], hydro- and solvothermal methods [4],

precipitation method [3, 16], microemulsion [7], and microwave method [2, 6]. N.T. Huong et al. in [6] obtained the nanowires/nanorods of europium/terbium monohydrate orthophosphate with Eu^{3+} concentrations of 6–20 at.%, with a length of 150–300 nm and a width of 10–50 nm, by microwave synthesis. Nano- and micro-powders of YPO_4 and $LuPO_4$ doped with Nd^{3+} activated by the different concentrations of Nd^{3+} ions (1–7 mol.%) were synthesized by hydrothermal method and solid-state reaction at high temperature [4]. The synthesis method using microwave radiation is used because of the high probability of forming the low-dimensional nanomaterials in a simple, fast, efficient, and non-toxic way. Documented in [2] YPO_4 and (Y,Ln)PO_4 (Ln = Eu, Tb, Dy, Ho, Tm, Ce, and Eu/Tb) tetragonal phosphate hydrates have been synthesized by microwave-assisted processing. The polycrystalline spheres ($\sim$ 0.7–1.5 μm in diameter) consisted of confined 10–17 nm nanocrystals.

A. Tymiński et al. [1] report about $REPO_4$ (RE = Y^{3+}, La^{3+}, Gd^{3+}, and Lu^{3+}) nanoparticles doped with Ho^{3+}, Er^{3+}, Tm^{3+}, Tb^{3+}, and Yb^{3+} ions which show intense upconversion luminescence. The authors believe that the studied $REPO_4$ matrices are good for the upconversion of Ln^{3+} ions; Tb^{3+} and Yb^{3+} ions were sensitizing ions, and Ho^{3+}, Er^{3+}, Tm^{3+}, Tb^{3+} — emitter ions [1]. The medium sizes of the lutetium phosphate nanoparticles were 22, 34, 74–77 nm. These samples exhibited strong luminescence upon excitation in the near-IR range (975–978 nm). The samples luminesced in the wavelength range 475–688 nm, depending on the dopant ion, when excited at 978 nm.

The use of an ion pair Nd^{3+}–Pr^{3+} to create the ultraviolet emitting nanoscale scintillators based on the nanosized particles of lutetium phosphate for the purpose of their further use during radiation therapy is presented in [19]. The authors propose the use of Nd^{3+} ions as a dopant for $LuPO_4$:Pr^{3+} nanoparticles in order to increase the ultraviolet C (UV-C) emission upon X-ray excitation. The authors state that the presence of Nd^{3+} ions promotes an increase in radiation intensity due to the energy transfer from Nd^{3+} to Pr^{3+}. In [20], the upconversion emission from Nd^{3+} ions in the UV/blue region and the energy transfer from Nd^{3+} ions to Pr^{3+} ions has been observed in a tellurite glass upon excitation at 532 nm.

The aim of our work was to investigate the influence of dopants and the regime of syntheses on the formation of non-agglomerated ($LuPO_4$:Pr,Nd) nanocrystals and microcrystals. Structural and morphological qualities of the manufactured orthophosphates have been confirmed and examined utilizing the X-ray diffraction (XRD) and transmission electron microscopy (TEM) methods. The effect of luminescent ions concentration on the optical properties, energy transfer phenomena, and excited states relaxation dynamic was studied within a wide spectral region. Further use of such materials as effective phosphors was verified by studying in detail their morphology, optical properties, and host–activator and Nd–Pr interplays.

2. Experimental details

2.1. Synthesis

The single-phase Pr and Nd-doped $LuPO_4$ nanocrystals were synthesized by the microwave hydrothermal method. The reagents Lutetium(III) oxide Lu_2O_3 (99.99%, REaton*), Pr_2O_3 (99.9%, Chem PUR), Nd_2O_3 (99.99%, REacton), HNO_3 (65%, pure P.A., POCH Basic), and H_3PO_4 (85%, P.A. POCH) acids and ethylene glycol (> 99.0%, Chemat) were used as the precursors. The synthesis of lutetium phosphate nanocrystals (NCr $LuPO_4$) was carried out similarly to that described in [2] for yttrium phosphate nanoparticles. Pr_2O_3 and Nd_2O_3 were preliminarily dissolved in a solution of nitric acid diluted three times with distilled water until complete dissolution, and then the solutions were evaporated to remove excess acid at a temperature of $\sim$ 85°C. After that, the solutions were transferred into the flasks and made up to the mark with distilled water. In the case of Lu_2O_3, the oxide was dissolved in nitric acid using a microwave reactor, and then excess of the acid was removed by evaporation. The RE precursors were added to the container, urea was added (18 mol per 1 mol $(RE)_2O_3$, where RE = Lu^{3+}, Pr^{3+}, Nd^{3+} ions), ethylene glycol (1/4 of the total volume of the solution) was added and stirred for 10–20 min, then CTAB was added (2 mol per 1 mol $(RE)_2O_3$, where RE = Lu^{3+}, Pr^{3+}, Nd^{3+} ions), stirred until complete dissolution, and then excess of the phosphoric acid was added. Urea was added to the reaction mixture to reduce the acidity of the solution, as reported in [21].

After that, the mixture was stirred for 30–40 min and placed in a microwave hydrothermal reactor. The synthesis was carried out for 20 min, first at 100°C and then at 80°C. After that, the synthesized precipitate was washed several times in distilled water and dried at 50°C for 24 h. Annealing was carried out at 1000°C, and then, in some cases, also at 1200°C as in [2, 3]. $Lu_{1-x-y}Pr_xNd_yPO_4$ nanocrystals were synthesized, achieving the single-doped samples at the concentration of Pr^{3+} of 0, 0.5, 1.5, 2.0%, and the co-doped orthophosphates containing Nd^{3+} (1, 2, 3%) — at Pr^{3+} concentration of 1%.

A sample of NCr $LuPO_4$:1%Pr, 3%Nd was also synthesized for comparison by precipitation using components in the same proportions as in a microwave hydrothermal synthesis and using CTAB.

In addition, $Lu_{1-x-y}Pr_xNd_yPO_4$ polycrystals were also synthesized by the solid-state reaction technique from mixtures of the stoichiometric amounts of starting materials. $LuPO_4$:Pr,Nd was

synthesized using $NH_4H_2PO_4$. All precursors were weighed in the required proportions, placed in an agate mortar, and thoroughly ground. Then, annealing was carried out consistently at temperatures of 800, 1000, and 1300°C for 12 h, as described in [4]. After each stage of annealing, the samples were ground again in an agate mortar.

2.2. Measurements

The resulting nano and microcrystals were characterized by applying the X-ray diffraction method, TEM measurements, and optical spectroscopy techniques. The phase purity of the samples was verified by XRD (X'Pert PRO PANalytical diffractometer, non-monochromatized CuK_α radiation) with the Match!3 program used for the display and analysis of the diffractograms. The measurements were carried out in the 2θ range of 10–100° with a scanning rate of 2θ min^{-1}.

The morphology of the NCr $LuPO_4$ samples was determined by transmission electron microscopy (TEM), using a Philips CM-20 SuperTwin instrument operating at 160 kV.

The ultraviolet-visible (UV-Vis) emission and excitation spectra were recorded utilizing an FLS1000 fluorescence spectrometer (Edinburgh Instruments) equipped with a 450 W xenon lamp as an excitation source and a Hamamatsu 928 photomultiplier. The vacuum ultraviolet (VUV) spectra were measured applying a McPherson monochromator, and near-infrared emission spectra were recorded by means of an Optron DM711 monochromator (Dong-Woo Optron Co. Ltd., Kyungg-do, Korea) with a 750 mm focal length and a Hamamatsu InGaAs detector. Decay curves of Pr^{3+} and Nd^{3+} ions luminescence were acquired utilizing an experimental set-up consisting of a Continuum Surelite optical parametric oscillator (OPO) pumped by the third harmonic of a Nd:YAG laser, a GDM 1000 double grating monochromator, R3896 Hamamatsu photomultiplier, and a Tektronix MDO-40-54-B–3 Mixed Domain Oscilloscope.

3. Results and discussion

3.1. XRD analysis

The absence of other phases in the synthesized (NCr) $Lu_{1-x-y}Pr_xNd_yPO_4$ samples (0–2% Pr^{3+} at 0% Nd^{3+}; and 1, 2, 3% Nd^{3+} at 1% Pr^{3+} ions in the solutions) was determined using the X-ray powder diffraction (XRD) method. The X-ray diffraction patterns of both pure NCr $LuPO_4$ nanocrystals and those doped with Pr^{3+} and Nd^{3+} ions, annealed at $T = 1000$°C, are shown in Fig. 1a, b, and confirm the formation of the pure phase orthophosphates. The position of the diffraction peaks on the X-ray patterns indicates that they correspond to the standards of the tetragonal system (Space group I 41/a m d Z (141)) attributed to the ICSD-162336 data (Inorganic Crystal Structures Database). The introduction of Pr^{3+} ions at a concentration of up to 2% and Nd^{3+} ions at a concentration of up to 3% does not lead to a violation of the $LuPO_4$ crystal structure. The XRD diffraction patterns of Pr^{3+} and Nd^{3+}-doped $LuPO_4$ indicate the formation of 99.8–100% $LuPO_4$.

TABLE I

The sizes of (NCr) $LuPO_4$ doped with 0–2% Pr^{3+} and 0–3% Nd^3 obtained from XRD data (Figs. 1, 2) and TEM images (Figs. 3–5).

Sample	Nanocrystal size (XRD) [nm]	Nanocrystal size (TEM)[a] [nm]	Crystal lattice parameter, a [Å]	Crystal lattice parameter, c [Å]
NCr $LuPO_4$	34.5 ± 4	30–50	6.80085	5.96333
NCr $LuPO_4$:0.5%Pr	37.3 ± 5	40–70	6.79736	5.96125
NCr $LuPO_4$:1%Pr	32.8 ± 5	40–80	6.79911	5.96251
NCr $LuPO_4$:2%Pr	33.4 ± 3	40–70	6.79846	5.96268
NCr $LuPO_4$:1%Pr, 1%Nd	34.8 ± 5	40–70	6.79904	5.96387
NCr $LuPO_4$:1%Pr, 2%Nd	34.2 ± 4	40–90	6.79691	5.96104
NCr $LuPO_4$:1%Pr, 3%Nd	35.1 ± 4	40–90	6.79675	5.96235
NCr $LuPO_4$:1%Nd	36.3 ± 1	–	6.80002	5.96516
NCr $LuPO_4$:1%Pr, 3%Nd[b]	36.9 ± 5	–	6.79632	5.96401
NCr $LuPO_4$, without CTAB	37.4 ± 6	30–50	6.79815	5.96122
NCr $LuPO_4$, without CTAB (1200°C)[c]	43.2 ± 6	80–160	6.80006	5.96238

[a]The measurement of nanocrystals was along their long side

[b]The sample was synthesized by the precipitation method and annealed at 1000°C

[c]The sample was fabricated by the microwave hydrothermal method and annealed at 1200°C;
all other samples were synthesized by the microwave hydrothermal method and annealed at 1000°C

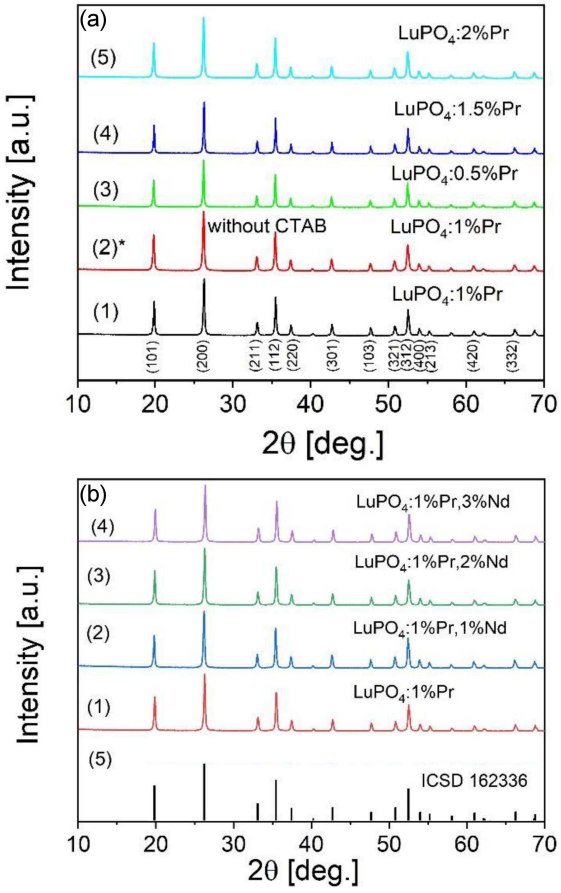

Fig. 1. XRD patterns of (NCr) $Lu_{1-x-y}Pr_xNd_yPO_4$ synthesized with different concentrations of Pr^{3+} and Nd^{3+} ions in the solutions. The samples 1, 3–5 (a) and 1–4 (b) were prepared with CTAB, but the sample 2*(a) – without CTAB. The samples were annealed at 1000°C. The "ICSD 162336" spectrum of $LuPO_4$ — spectrum 5.

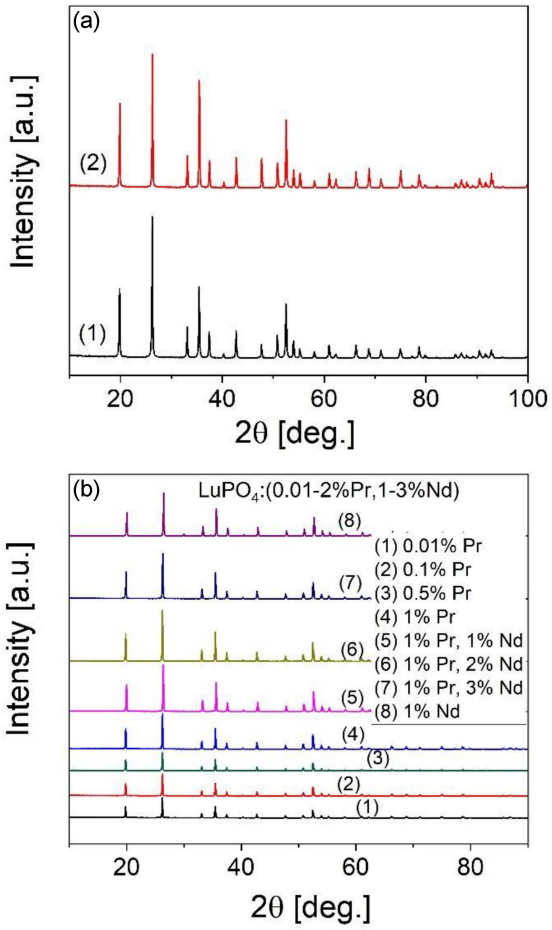

Fig. 2. XRD patterns of (a) (NCr) $LuPO_4$ synthesized without CTAB and annealed at 1000°C (1) and 1200°C (2); (b) $LuPO_4$:Pr:Nd microcrystals synthesized by a solid-state method.

It should be noted that the addition of organic CTAB molecules during the synthesis of the samples did not affect the formation of the crystalline phase of the lutetium phosphate (Fig. 1). For samples synthesized using CTAB, the diffraction patterns were as narrow as for pure samples (Fig. 1a, the diffraction pattern 2*). The lattice parameters calculated from the diffractograms are within the limits $a = 6.79736$–6.79800 Å, $b = 5.96125$–5.96516 Å for doped samples (Table I; see also Figs. 1 and 2). Determined values are close to $a = 6.792(2)$ Å, $b = 6.792(2)$ Å, $c = 5.955(2)$ Å taken from [22], and $a = 6.7917(3)$ Å, $b = 6.7917(3)$ Å, $c = 5.9524(3)$ Å given in [23] for the nano-sized $LuPO_4$:Pr^{3+} (0.1 at.%) phosphor powders synthesized by a sol–gel process.

The position and width of the peaks in the diffraction patterns of the pure $LuPO_4$ nanocrystals annealed first at 1000°C and then at 1200°C are similar (Fig. 2a). This indicates that the selected annealing temperature of 1000°C is sufficient to obtain samples of doped lutetium phosphate nanocrystals, both non-agglomerated and with good crystallinity.

The measured XRD spectra of (NCr) $LuPO_4$ samples doped with Pr^{3+} and Nd^{3+} ions (single-doped 0.5–2% Pr^{3+}; co-doped 1, 2, 3% Nd^{3+} and 1% Pr^{3+}) showed that the positions of peaks are similar, but the peaks are somewhat broadened compared to the XRD peaks of $LuPO_4$:Pr:Nd microcrystals synthesized by a solid-state method (Fig. 2b). This is due to the smaller crystallite size and crystallinity [24] of (NCr) $LuPO_4$.

It should be noted that the width of the diffraction peaks was narrower for the samples obtained by the solid-state method (with the introduction of Pr^{3+} and Nd^{3+} ions in the concentrations similar to those in the synthesis of nanocrystals by means of the hydrothermal method) and annealed at 1200°C (compared to the microwave hydrothermal method) (Fig. 2b). The higher crystallinity and larger particle size can be discerned in samples obtained by a solid-state reaction in relation to particles obtained by the hydrothermal microwave method.

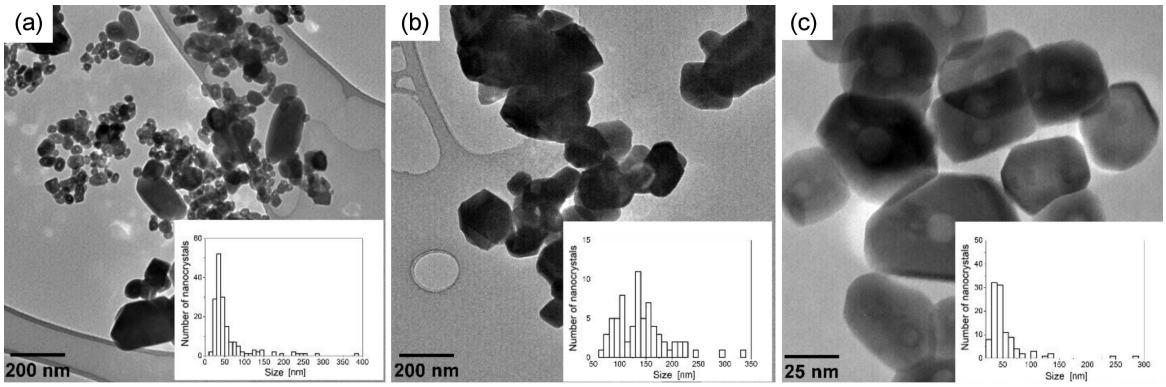

Fig. 3. TEM images of the pure (NCr) $LuPO_4$ (a–c) and histograms of their distribution (in the insets). The sample of (NCr) $LuPO_4$ was synthesized without CTAB and annealed at 1000°C (a) and after that at 1200°C (b). The sample in (c) was synthesized with CTAB and annealed at 1000°C.

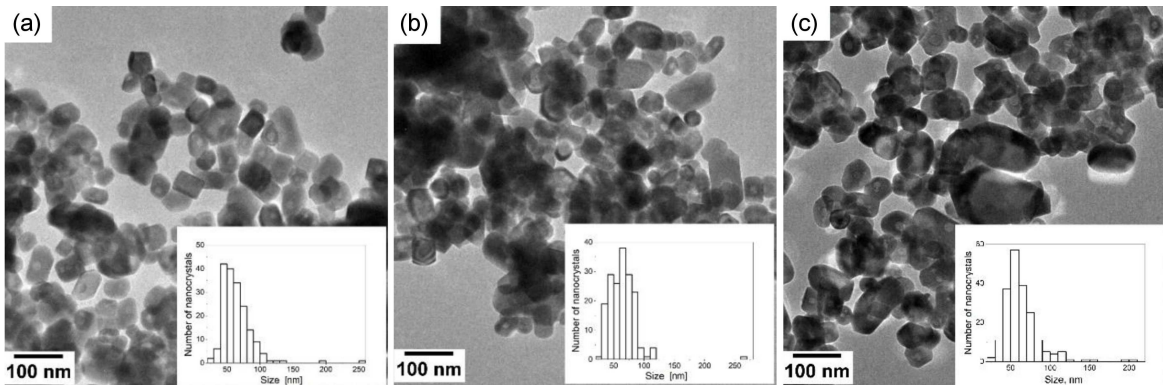

Fig. 4. TEM images of $LuPO_4$:Pr nanocrystals with different concentration of Pr^{3+} (0.5% (a), 1% (b), 2% (c)) in the solution. The samples were synthesized with CTAB and annealed at 1000°C.

The classical Scherrer method was used to calculate the size of (NCr) $Lu_{1-x-y}Pr_xNd_y(PO_4)$ obtained by the microwave hydrothermal method. The nanocrystal size was calculated using the formula given in [2]

$$D_{hkl} = \frac{K\lambda}{B\cos(\theta)}, \tag{1}$$

where D is the crystallite size; λ is the X-ray wavelength; B is the peak width of the diffraction peak profile at half maximum height; θ is the Bragg angle; K — Scherrer's constant, due to the shape of the crystallite ($K = 0.94$ for crystalline form as in [25–27] since most nanocrystals were cube-shaped).

The crystallite sizes were estimated from the diffraction patterns shown in Fig. 1. They were within 31–37 nm (for the lutetium phosphates synthesized with CTAB) and 40.2–40.4 nm for the samples synthesized without CTAB. An increase in the annealing temperature from 1000 to 1200°C leads to the coarsening of the crystallites from 40.4 to 43 nm (XRD data, Table I) for the exemplary sample of $LuPO_4$ synthesized without CTAB and containing the rare earth ions as dopants.

3.2. Morphological qualities

The study on the morphology of (NCr) $LuPO_4$ samples (synthesized without CTAB) by TEM method showed their significant coarsening with an increase in the annealing temperature from 1000°C (30–50 nm in the main and a few of 100–450 nm) to 1200°C (80–160 nm in the main and a few of 200–300 nm) (Fig. 3a). In addition, agglomeration of the nanocrystals was observed as a result of annealing at 1200°C (Fig. 3b), which also leads to a significant nonuniformity of the crystal sizes and is not a good property for obtaining homogeneous material. The introduction of CTAB into the reaction mixture leads to the formation of particles of a more regular single-crystal shape, and large particles are mostly absent, i.e., the size of nanocrystals is mainly 30–50 nm, however, there are also particles with a size of 100–250 nm (Fig. 3c).

The single crystallinity of the form of the lutetium phosphate samples, both pure and with the addition of Pr^{3+} and Nd^{3+} ions, synthesized by the microwave hydrothermal method was confirmed by studying their morphology. As can be seen from

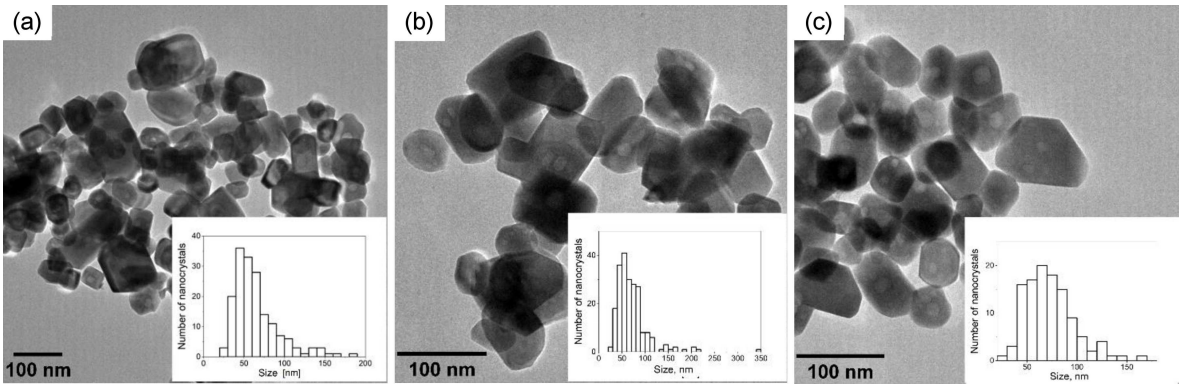

Fig. 5. TEM images of $LuPO_4$:1%Pr (1–3%Nd) nanocrystals with the concentration of Nd^{3+} (1% (a), 2% (b), 3% (c)) in the solution. The samples were synthesized with CTAB and annealed at 1000°C.

the TEM photo and inset histograms, the size of lutetium phosphate nanocrystals was mainly 40–70 nm for nanocrystals synthesized with 0.5–2% Pr^{3+} and 1% Nd^{3+} at 1% Pr^{3+} when using CTAB (Table I). In this case, a certain amount of particles with a size of 110–250 nm is also formed, but its proportion does not exceed 10–15%. However, with an increase in the concentration of Nd^{3+} ions in the solution to 2–3% (at 1% Pr^{3+}), the size of nanocrystals increases to an average value of 40–90 nm (Figs. 4, 5).

A similar rise in the crystal size with an increase in the Nd^{3+} ions concentration upon doping with YPO_4 and $LuPO_4$ was described in [4]. In the case of YPO_4, the particle size was about 20–25 nm (1% Nd^{3+}), 40–45 nm (3%), 25–30 nm (5%), and 30–35 nm (7%), and in the case of $LuPO_4$, there was some increase in the size of crystallites, i.e., to 30 nm (1% and 3% Nd^{3+}) and 40–50 nm (5% and 7%). The increase in the size of nanocrystals that we also observed upon the introduction of Nd^{3+} ions at the concentrations of 2 and 3% as a doping impurity compared to its concentration of 1% is probably due to the features of crystallization in the presence of these ions.

Relevant properties of trivalent rare earth ions and their isomorphism contribute to their uniform distribution in nanocrystalline particles and are described in [2]. Accordingly, well-dispersed homogeneous YPO_4 spheres with a diameter of ~ 0.7–1.5 μm were obtained in [2] by microwave-assisted processing with the addition of rare-earth elements. The authors of [2] obtained polycrystalline spheres consisting of the nanocrystals 10–17 nm in size. The spherical shape and dispersion of the initial particles were well preserved up to a temperature of 1000°C. It was shown that the shape of YPO_4:RE^{3+} nanocrystals depends on a large extent of surface adsorption. Yttrium orthophosphate crystallized within a few minutes into submicron and micron spheres due to its extremely low solubility in water (solubility product from 10^{-25} to 10^{-27}).

The measurement was carried out only along the long side of the nanocrystals in order to take into account the growth of the nanocrystal along one of the sides. The particle sizes measured using TEM are generally in the range from 30 to 90 nm (for samples annealed at 1000°C). At the same time, it should be noted that the sizes of crystallites determined by XRD for the same samples are in the range of 31–40 nm (Table I). The difference in the estimated sizes of crystallites from the TEM and diffraction data can be due to the features of the measurements.

Urea was used in the synthesis of $LuPO_4$ nanocrystals by the microwave hydrothermal method, which contributed to raising the pH of the solution to pH 2.5–3. Nanocrystalline particles of lutetium phosphate with the addition of active ions were synthesized by microwave hydrothermal synthesis. The addition of ethylene glycol and CTAB to an aqueous solution will help limit the growth of crystals in the reactor due to the adsorption of a surfactant onto the surface of the growing faces.

Changing the mode of preparation of particles affects their size and shape. The use of the precipitation method leads to the formation of particles with a similar size as those obtained by the microwave hydrothermal method, however, both individual particles and conglomerates of particles appear. Increasing the synthesis time leads to the formation of a higher number of large particles, however, the shape of the particles changes, becomes more rounded, and the number of them with the correct shape decreases. The resulting crystals become less faceted, their average size is 60–100 nm, while round-shaped crystalline particles 300–500 nm in size are also formed.

It is known that the growth of micro and nanocrystals in solution is significantly affected by adsorption on the surface of growing faces of various ions or organic molecules from the solution. As such, we chose CTAB, which has a positive charge on one side and a long hydrocarbon chain on the other. The addition of the organic solvent ethylene glycol to the

reaction mixture promotes good dissolution of the CTAB molecules as well. Furthermore, the presence of ethylene glycol in the reaction mixture promotes faster crystallization of lutetium phosphate.

3.3. Luminescent properties

Luminescent properties of the nanocrystalline and microcrystalline $LuPO_4$ orthophosphates doped with Pr^{3+} and Nd^{3+} ions synthesized respectively by the microwave hydrothermal method have been verified and compared within the different spectral regions. The involved phenomena can be referenced to the Pr^{3+} and Nd^{3+} ions energy levels scheme presented in Fig. 6. The radiative transitions are described as the solid arrows, whereas the dashed lines are assigned to the nonradiative processes.

The co-doped (Pr + Nd) and single-doped samples have been excited in the effective Pr^{3+} ions absorption bands ${}^3H_4 \rightarrow {}^3P_J$ at 445 nm and Nd^{3+} ions ${}^4I_{9/2} \rightarrow {}^4F_{5/2}, {}^2H_{9/2}$ at 803 nm. As it has been recently presented by Pawlow et al. [4], no absorption band around 445 nm exists in $LuPO_4$:Nd, and accordingly, these aforementioned excitation wavelengths enable selective excitation of the involved optically active ions. It can be well discerned in Fig. 7b that the near-infrared emission of Pr^{3+} ions in the single-doped microscale sample manifests itself actually by two bands attributed to the transitions ${}^3P_0 \rightarrow {}^1G_4$; ${}^1D_2 \rightarrow {}^3F_{3,4}$ (950–1120 nm) and ${}^1D_2 \rightarrow {}^1G_4$ (1330–1550 nm).

In the case of the co-doped $LuPO_4$:Pr,Nd microscale orthophosphates, optical excitation at 445 nm is effectively transferred from ${}^3P_J$ Pr^{3+}

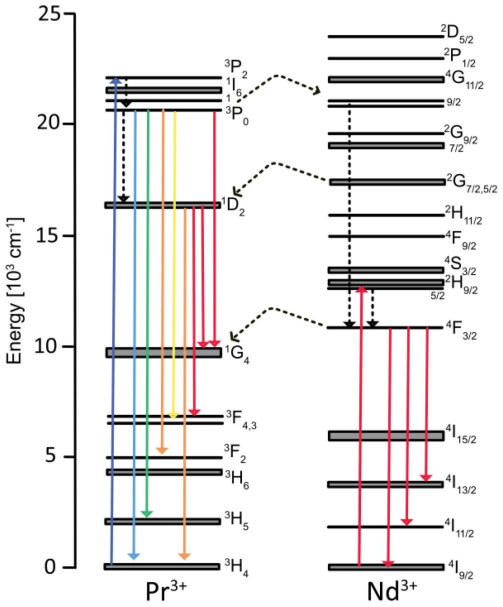

Fig. 6. Energy levels scheme of Pr^{3+} and Nd^{3+} in lutetium orthophosphate.

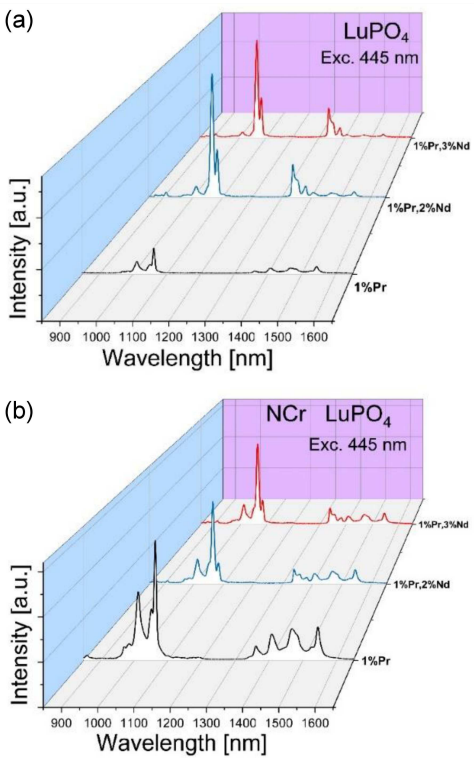

Fig. 7. NIR emission spectra of nano (b) and microcrystalline (a) $LuPO_4$ excited at 445 nm recorded for Pr single-doped and Pr + Nd co-doped $LuPO_4$.

manifolds to neighboring Nd^{3+} ions activators, and as a result, the intense NIR emission bands at 1064 nm and 1350 nm occur. These observed intense emission bands correspond to the transition from a metastable ${}^4F_{3/2}$ Nd^{3+} manifold to the lower energy ${}^4I_{11/2}$ and ${}^4I_{13/2}$ states, respectively. The efficiency of NIR Nd^{3+} ions emission increases for higher concentration of Nd^{3+} in the co-doped samples. Quite different features of the near-infrared emission have been acquired for nanocrystalline (NCr) orthophosphates excited at 445 nm. Figure 7b reveals that near-infrared emissions studied for the single-doped (Pr^{3+}) and co-doped (Pr^{3+} + Nd^{3+}) NCr orthophosphates are efficient in both NIR spectral regions. The impact of the neodymium admixture on the observed NIR luminescence is weaker in relation to the microscale orthophosphates, and especially intense neodymium luminescence appears at 1064 nm in these co-doped samples.

Figure 8 displays the comparison of the near-infrared emission spectra recorded for (NCr) and micro-scaled Nd^{3+} single-doped and Nd + Pr co-doped orthophosphates excited at 803 nm directly into ${}^4I_{9/2}$–${}^4F_{5/2}$+${}^2H_{9/2}$ absorption band of Nd^{3+}.

It can be seen that near-infrared emission bands of Nd^{3+} ions corresponding to ${}^4F_{3/2}$–${}^4I_{9/2}$, ${}^4F_{3/2}$–${}^4I_{11/2}$, and ${}^4F_{3/2}$-${}^4I_{13/2}$ transitions are significantly diminished for samples co-doped with Pr^{3+} ions. Integrated luminescence of Nd^{3+} ions intensity

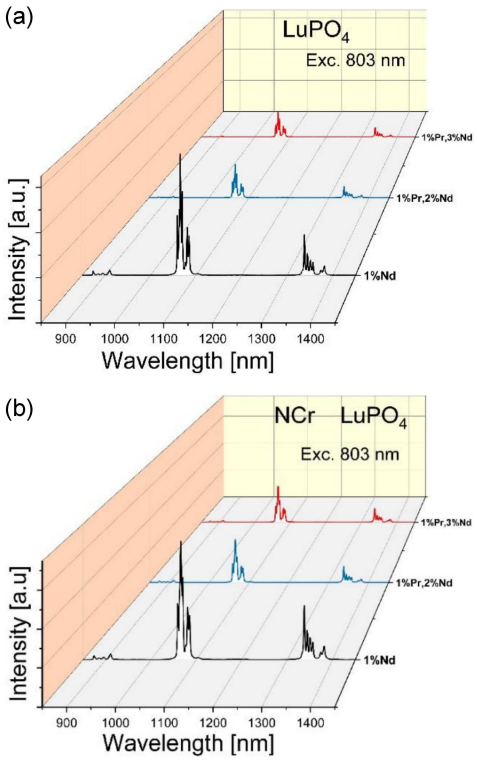

Fig. 8. NIR emission spectra of nano (b) and microcrystalline (a) $LuPO_4$ excited at 803 nm recorded for Nd single-doped and Pr + Nd co-doped $LuPO_4$.

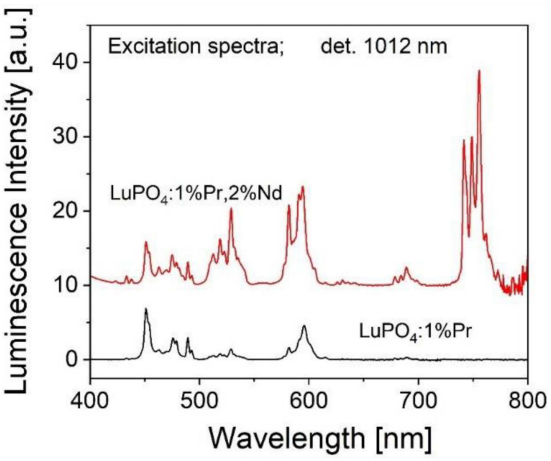

Fig. 9. Excitation spectra of Pr^{3+} ions luminescence monitored at 1012 nm and measured for $LuPO_4$:1%Pr and $LuPO_4$:1%Pr, 2%Nd nanocrystals.

determined for the co-doped $LuPO_4$:1%Pr, 3%Nd is reduced by a factor of 3.5 in relation to single-doped micro-scaled $LuPO_4$:1%Nd. This quenching process is quite effective for nanocrystalline orthophosphates as well, and integrated luminescence of Nd^{3+} ions intensity is 2.8 times lower in NCr co-doped sample compared to single-doped $LuPO_4$:1%Nd. The near-infrared luminescence is

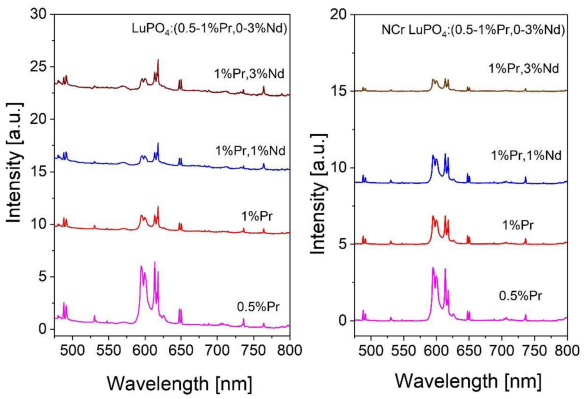

Fig. 10. Emission spectra of micro and nanosized $LuPO_4$ doped with Pr^{3+} ions and co-doped with Nd^{3+} ions excited at 451 nm.

lowered as a result of the concentration quenching process associated with the Nd–Nd interactions, but nevertheless, the contribution of phonon-assisted $Nd(^4F_{3/2})$–$Pr(^1G_4)$ energy transfer can be considered as well. Actually, the achieved spectroscopic results in the spectral range of 970–1450 nm indicate that the effective energy transfer between optically active ions occurs in samples $Lu_{1-x-y}Pr_xNd_yPO_4$ synthesized by both the solid-state and microwave hydrothermal methods.

The Nd–Pr energy transfer was verified by analyzing the excitation spectra of Pr^{3+} ions luminescence in the single-doped and co-doped samples, which are displayed in Fig. 9. The monitored luminescence line 1012 nm is solely attributed to Pr^{3+} luminescence, since the $^4F_{3/2}$–$^4I_{11/2}$ emission band of Nd^{3+} ions arises scarcely at 1045 nm. The excitation spectrum of Pr^{3+} luminescence recorded for a single-doped sample consists of bands corresponding to $^3H_4$–^3P_J and $^3H_4$–$^1D_2$ Pr^{3+} transitions. In the case of the co-doped $LuPO_4$:1%Pr, 2%Nd orthophosphates, an adequate excitation spectrum contains the additional lines located especially within 500–550 nm and 730–780 nm spectral regions. These prominent bands are attributed to neodymium transitions $^4I_{9/2}$–$^2K_{13/2}$ + $^4G_{7/2}$ + $^4G_{9/2}$ and $^4I_{9/2}$-$^4S_{3/2}$+$^4F_{7/2}$ confirming the contribution of Nd^{3+} ions in activation of Pr^{3+} emission in the studied orthophosphates.

A comparison of the visible Pr^{3+} ions luminescence excited at 451 nm in nano/micro-scaled $LuPO_4$:Pr and $LuPO_4$:Pr,Nd is shown in Fig. 10. Emission spectra were recorded for various concentrations of the luminescent ions. Spectral characteristics of measured emission bands are rather unchangeable when analyzing single-doped and co-doped samples. Most intense bands are associated with $^1D_2$–$^3H_4$ praseodymium transitions and manifest themselves by intense peaks at 618 nm, while blue emission originating in the $^3P_0$ manifold is rather ineffective, and as a result, two weak peaks can be seen at 488 nm and 491 nm.

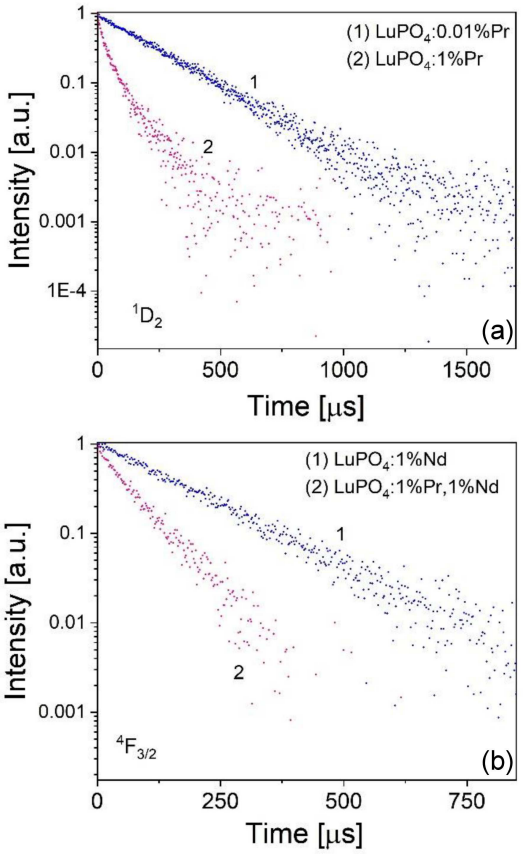

Fig. 11. Decay curves of (a) $^1D_2$ Pr^{3+} and (b) $^4F_{3/2}$ Nd^{3+} ions luminescence recorded for $LuPO_4$:Pr and $LuPO_4$:Pr,Nd samples.

TABLE II

Experimental lifetimes of luminescent levels in $LuPO_4$:Pr,Nd.

Sample	Experimental lifetime [μs]		
	$^3P_0$ (Pr)	$^1D_2$ (Pr)	$^4F_{3/2}$ (Nd)
$LuPO_4$:0.01%Pr	0.51 ± 0.004	220 ± 0.25	–
$LuPO_4$:0.1%Pr	0.51 ± 0.005	218 ± 0.32	–
$LuPO_4$:0.5%Pr	0.56 ± 0.004	208 ± 0.48	–
$LuPO_4$:1%Pr	0.55 ± 0.003	38 ± 0.23	–
$LuPO_4$:1%Nd	–	–	160 ± 0.22
$LuPO_4$:1%Pr, 1%Nd	0.54 ± 0.005	31 ± 0.26	76 ± 0.27
$LuPO_4$:1%Pr, 2%Nd	0.50 ± 0.005	23 ± 0.23	48 ± 0.18
$LuPO_4$:1%Pr, 3%Nd	0.51 ± 0.005	22 ± 0.24	40 ± 0.17

In order to get more insight into energy transfer phenomena between Pr^{3+} and Nd^{3+} ions in the lutetium orthophosphates, the experimental lifetimes of the luminescent levels have been studied for the single-doped and co-doped samples. As is presented in Table II, the lifetime of the $^3P_0$ excited state is not actually varied for all studied samples, and experimental lifetimes have been estimated to be 0.5 μs. The opposite effect has been found for the lower-energy $^1D_2$ praseodymium excited state that is effectively quenched in orthophosphates doped with higher concentrations of Pr^{3+} ions. For instance, the experimental lifetimes of 220 μs were measured for $LuPO_4$:0.01%Pr, and this value was significantly reduced to 38 μs for $LuPO_4$:1%Pr. The single exponential decay curve of $^1D_2$ luminescence is displayed in Fig. 10 for the diluted sample, while the nonexponential decay occurs for $LuPO_4$:1%Pr. The cross-relaxation channels are responsible for the reduction of $^1D_2$ lifetimes in single Pr^{3+}-doped samples, and a further shortening of these lifetimes in co-doped orthophosphates is the result of Pr–Nd inter-ionic interactions. Eventually, the $^1D_2$ experimental lifetime is roughly two-fold lowered to 22 μs when the sample contains 3% Nd^{3+} ions and 1% Pr^{3+} ions.

The effect of co-doping of Nd^{3+} ions on a relaxation dynamic of $^1D_2$ excited state of Pr^{3+} ions can be clearly perceived. The impact of Pr^{3+} on Nd^{3+} ions luminescence decay in $LuPO_4$:Pr,Nd is efficient as well. Figure 11b displays exponential decay curves of $^4F_{3/2}$ Nd^{3+} luminescence measured for $LuPO_4$:1%Nd and $LuPO_4$:1%Pr, 1%Nd. The values of the estimated experimental lifetimes of Nd^{3+} ions luminescent levels are listed in Table II. Thus, the 52% reduction of $^4F_{3/2}$ experimental lifetime is attributed to co-doped $LuPO_4$:1%Pr, 1%Nd sample compared to Nd^{3+} ions in $LuPO_4$:1%Nd single-doped sample. In fact, the excitation energy is considerably transferred from Pr^{3+} to Nd^{3+} ions, and the next backward Nd–Pr energy transfer may take place. Consequently, the contribution of nonradiative processes to the relaxation of luminescent levels of Pr^{3+} and Nd^{3+} ions is heightened by substantial ion–ion interactions in the co-doped orthophosphates.

4. Conclusions

The influence of luminescent dopants (Pr + Nd) and synthesis conditions on the formation of $LuPO_4$ nano and microcrystals was studied and verified. $Lu_{1-x-y}Pr_xNd_yPO_4$ phosphate were obtained in the form of polycrystals by solid-state reaction technique and in the nanocrystalline form by the microwave hydrothermal method. The XRD patterns of Pr^{3+} and Nd^{3+}-doped $LuPO_4$ indicate that all diffraction peaks remain in accordance with the standards corresponding to the tetragonal system of $LuPO_4$. It was found that the incorporation of the luminescent ions Pr^{3+} and Nd^{3+} at their concentrations below 3 at.% does not lead to initiating any structural modification of the obtained $LuPO_4$ nano and polycrystals. The $Lu_{1-x-y}Pr_xNd_yPO_4$ ($x = 0.5$–2%; $y = 1$–3%) nanocrystals were of a size of 40–90 nm and their shape has the single-crystal morphology. The addition of CTAB results in the appearance of particles with a more regular crystalline shape in contrast to the synthesis without CTAB.

The spectroscopic properties of nano and microcrystalline $LuPO_4$ orthophosphates doped with Pr^{3+} and Nd^{3+} ions have been studied within various spectral regions. In particular, the effective increase in near-infrared luminescence excited at 445 nm is observed in the co-doped orthophosphates $Lu_{1-x-y}Pr_xNd_yPO_4$ as a result of Pr^{3+}–Nd^{3+} energy transfer. Contrary, the decrease in the near-infrared luminescence intensity of the $Lu_{1-x-y}Pr_xNd_yPO_4$ samples is observed when neodymium $^4F_{5/2}$, $^2H_{9/2}$ states are directly excited at 803 nm. The relaxation dynamic of Pr^{3+} $^1D_2$ excited state is affected by Nd^{3+} co-doping, and backward Nd–Pr energy transfer can be considered as well, since the experimental lifetime of $^4F_{3/2}$ metastable level of Nd^{3+} ions is considerably reduced in the co-doped $LuPO_4$:Pr,Nd. Consequently, the contribution of nonradiative processes to the relaxation of the luminescent levels of Pr^{3+} and Nd^{3+} takes place due to significant ion–ion interactions in the co-doped orthophosphates.

The data presented in this study are openly available in Zenodo at https://doi.org/10.5281/zenodo.8272727.

Acknowledgments

This work was supported by the National Science Centre, Poland, under grant number DEC-2021/41/B/ST5/03792. This work was supported by the Polish Academy of Sciences by the through the program of support for scientists from Ukraine (PAS and NASU). The authors are grateful to N. Rebrova (Institute of Low Temperature and Structure Research PAS) for her help in processing the results of XRD.

References

[1] A. Tymiński, T. Grzyb, *J. Lumin.* **181**, 411 (2017).

[2] Q. Zhu, Z. Xu, Z. Wang, X. Wang, X. Li, X. Sun, J.-G. Li, *Cryst. Eng. Comm.* **20**, 3187 (2018).

[3] Z. Xu, Q. Zhu, X. Li, X. Sun, J.-G. Lid, *Mater. Res. Bull.* **110**, 149 (2019).

[4] J. Pawłów, K.A. Prokop, M. Guzik, Y. Guyot, G. Boulon, J. Cybinska, *J. Lumin.* **236**, 117997 (2021).

[5] X Wang, J. Shi, P. Li, S. Zheng, X. Sun, H. Zhang, *J. Lumin.* **209**, 420 (2019).

[6] N.T. Huong, N.D. Van, D.M. Tien, D.K. Tung, N.T. Binh, T.K. Anh, L.Q. Minh, *J. Rare Earths* **29**, 1170 (2011).

[7] S. Heer, O. Lehmann, M. Haase, H.-U. Gdel, *Angew. Chem. Int. Ed.* **42**, 3179 (2003).

[8] D. Wang, B. Xue, X. Kong et al., *Nanoscale* **7**, 190 (2015).

[9] M. Runowski, P. Woźny, I.R. Martín, V. Lavín, S. Lis, *J. Lumin.* **214**, 116571 (2019).

[10] L. Marciniak, A. Pilch, S. Arabasz, D. Jin, A. Bednarkiewicz, *Nanoscale*, **9**, 8288 (2017).

[11] S. Espinoza, M.-F. Volhard, H. Kätker, H. Jenneboer, A. Uckelmann, M. Haase, M. Müller, M. Purschke, T. Jüstel, *Part. Part. Syst. Charact.* **35**, 1800282 (2018).

[12] K.A. Prokop, M. Guzik, Y. Guyot, G. Boulon, M. Wilk-Kozubek, M. Sobczyk, A.-V. Mudring, J. Cybinska, *Mater. Sci. Eng. B* **275**, 115503 (2022).

[13] M. Runowski, A. Shyichuk, A. Tyminski, T. Grzyb, V. Lavín, S. Lis, *ACS Appl. Mater. Interfaces* **10**, 17269 (2018).

[14] M. Runowski, P. Woźny, I.R. Martin, *J. Mater. Chem. C* **9**, 4643 (2021).

[15] D. Wisniewski, S. Tavernier, A.J. Wojtowicz, et al., *Nucl. Instrum. Methods Phys. Res. A*, **486**, 239 (2002).

[16] Z. Zhang, R. Cao, L. Guo, P. Li, C. Liang, T. Li, *New J. Chem.* **42**, 15215 (2018).

[17] J.M. Nedelec, C. Mansuy, R. Mahiou, *J. Mol. Struct.* **651–653**, 165 (2003).

[18] L. Benharrat, L. Guerbous, D. Bradai, A. Boukerika, A. Manseri, N. Selmi, B. Rahal, M.S.E. Hamroun, *Thin Solid Films* **694**, 137738 (2020).

[19] S. Espinoza, M. Müller, H. Jenneboer et al., *Part. Part. Syst. Charact.* **36**, 1900280 (2019).

[20] K. Kumar, S.B. Rai, *Solid State Commun.* **142**, 58 (2007).

[21] K. Mongkolsuttirat, J. Buajarern, *J. Phys. Conf. Ser.* **1719**, 012054 (2021).

[22] G. Lohmüller, G. Schmidt, B. Deppisch, V. Gramlich, C. Scheringer, *Acta Cryst. B* **29**, 141 (1973).

[23] B. Kahouadji, L. Guerbous, D.J. Jovanovic, M.D. Dramicanin, A.H. Souici, *Opt. Mater.* **109**, 110252 (2020).

[24] J. Zou, Q. Zhu, X. Sun, J-G. Li, *J. Mater. Res. Technol.* **9**, 12052 (2020).

[25] K. Yadav, R. Sangwan, M. Barala, D. Mohan, S. Sanghi, *Mater. Today Proc.* **54**, 656 (2022).

[26] R.R. Prasanth, P. Manikandan, J. Muthukumar et al., *Mater. Today Proc.* **74**, 923 (2022).

[27] A.F. Qasrawi, S.Kh. Sulaiman, *Physica B* **646**, 414309 (2022).